Supplement of Atmos. Meas. Tech., 18, 6449–6464, 2025 https://doi.org/10.5194/amt-18-6449-2025-supplement © Author(s) 2025. CC BY 4.0 License.





Supplement of

The saturation vapor pressures of higher-order polyethylene glycols and achieving a wide calibration range for volatility measurements by FIGAERO-CIMS

Arttu Ylisirniö et al.

Correspondence to: Arttu Ylisirniö (arttu.ylisirnio@uef.fi)

The copyright of individual parts of the supplement might differ from the article licence.

S1 Conformer selection for COSMOtherm calculations

Due to memory limitations, it is not possible to include all of the conformers in COSMO*therm* calculations. The selection of the correct conformers is critical because different types of conformers can lead to several orders of magnitude variation in the estimated saturation vapor pressures (Kurtén et al., 2018; Li et al., 2023a). Previous studies have shown that conformers that are able to interact with the surrounding solution are energetically more favourable in the condensed phase than conformers containing intramolecular hydrogen bonds (Hyttinen & Prisle, 2020). In order to find the best agreement between our calculations and previous experiments, we tested multiple ways of selecting conformers for the calculation. First, we found a set of conformers using systematic conformer sampling and Merck molecular force field in the Spartan 20 program (Wavefunction Inc.). Because the large PEGs are flexible and have millions of possible conformers, we used the sparse systematic algorithm and limited the search to a small number of conformers. The number of searched conformers was reduced for the larger molecules in order to keep the computational cost of the calculations manageable. Additionally, the maximum number of searched conformers in the Spartan program is 2³⁰ (i.e., 2-fold rotations of 30 bonds) or 3¹⁹ (i.e., 3-fold rotations of 19 bonds). We therefore used only 2-fold torsions for the PEG- 6 to 14 and only the maximum 30 2-fold torsions were selected for PEG-12 and PEG-14. Table S1 shows the number of searched and found conformers for each of the PEG.

Table S1 - Conformer sampling details.

5

15

| n | # conformers searched | # conformers found |
|---------|-----------------------|------------------------|
| 5 | all | 21 891 |
| 6, 7, 8 | 20 000 | 14 293, 11 811, 12 491 |
| 10 | 10 000 | 6 349 |
| 12 | 5 000 | 3 403 |
| 14 | 1 000 | 674 |

All found conformers were optimized at the BP/def-TZVP level of theory using the TURBOMOLE program (TURBOMOLE, 2019). After the geometry optimization, duplicate conformers were removed with the CLUSTER_GEOCHECK algorithm of the COSMO*conf* program (BIOVIA - COSMOconf). Conformers with similar chemical potentials were omitted using the CLUSTER_MU algorithm. Additional higher-level single-point calculations were run at the BP/def2-TZVPD-FINE level of theory. The geometries of the chosen conformers were optimized at the BP/def-TZVP level of theory (gas phase), and the final gas-phase energies were calculated at the BP/def2-TZVPD level of theory.

The best agreement between experimental K2018 and COSMO-RS-derived saturation vapor pressures was found using the lowest pure compound chemical potentials calculated using the BP_TZVPD_FINE_21 parametrization. Using different

numbers of conformers in the COSMO*therm* calculations of PEGs 5-8 showed that the optimal conformer set contains all (up to 40) conformers that have negative pure compound chemical potentials (estimated using the BP_TZVPD_FINE-21 parametrization). For PEG-5 and PEG-6, only 4 and 2 conformers, respectively, remained after the removal of conformers with similar chemical potentials. Originally, 51 and 9 conformers with negative chemical potentials were found for PEG-5 and PEG-6, respectively. In order to have a sufficient number of conformers in the COSMO*therm* calculation, we included all conformers with negative chemical potentials in the pure compound (40 and 9) of PEG-5 and PEG-6.

The newer BP_TZVPD_FINE_21 parametrization gives between 1 to 3 orders of magnitude lower saturation vapor pressure estimates than the previous BP_TZVPD_FINE_20 parametrization. Better agreement with experiments was found using the BP_TZVPD_FINE_20 parametrization. The difference in the *P*_{sat} estimates is caused by differences in the chemical potentials between the two parametrizations. For example, the lowest chemical potential conformer has up to 2.4 kcal/mol higher chemical potential (and consequently condensed-phase free energy) in the BP_TZVPD_FINE_20 than in the BP_TZVPD_FINE_21 parametrization among the studied PEGs. The BP_TZVPD_FINE_21 parametrization systematically gives a wider range in chemical potentials than the previous BP_TZVPD_FINE_20 parametrization. This indicates that the new parametrization finds larger effects from structural differences, such as intramolecular hydrogen bonds, on the intermolecular interaction. Since the parametrization of COSMO*therm* has no effect on the gas-phase energy, the change in chemical potential is seen directly in the saturation vapor pressure value.

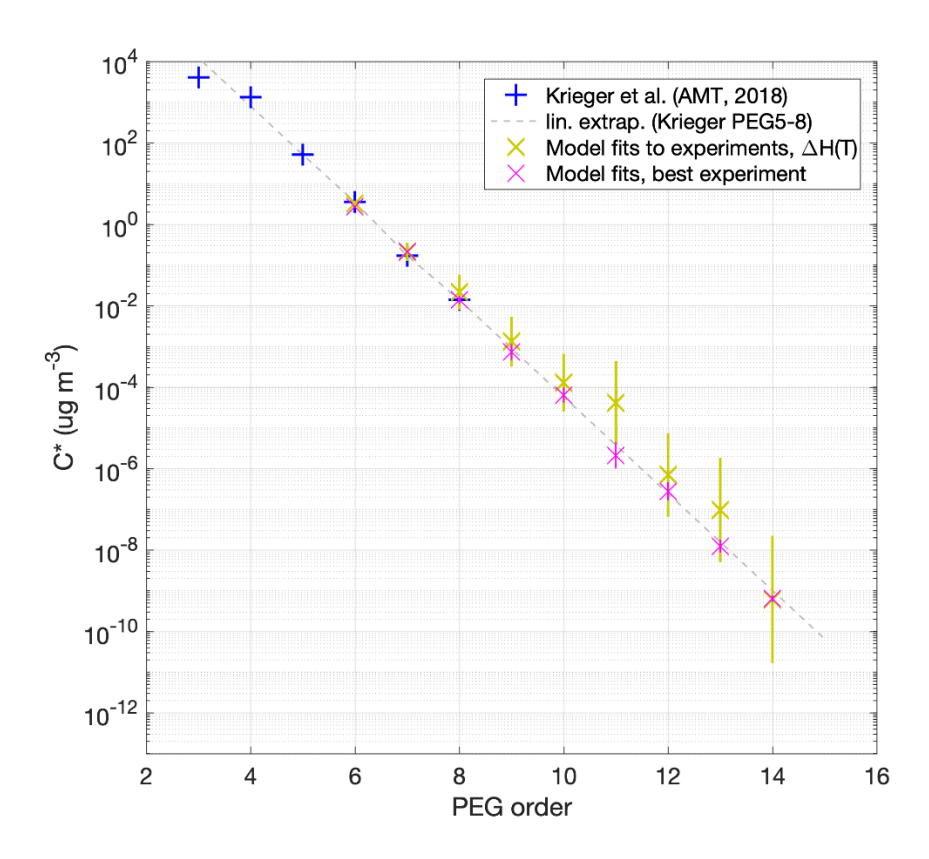


Figure S1: A more detailed look at the desorption model results for saturation vapor concentration at 298 K (C^* , in units of $\mu g m^{-3}$) as a function of PEG order (which is also directly proportional to mass). For reference, blue pluses are conversions from saturation vapor pressures reported in Krieger et al., (2018) for PEGs 3-8; the grey dashed line is an extrapolated linear fit to their values for PEGs 5-8. Yellow crosses are our results for PEGs 6-14, with uncertainties as vertical lines, from fitting the desorption model to a representative selection of three FIGAERO-CIMS experiments (as discussed in the main text and shown in Figures 1 and 3). Magenta crosses, also with uncertainties as vertical lines, are the results of the best-fitting experiment (described as "Experiment A" in the main text; uncertainties in this case correspond to the standard deviation, in logarithmic space, of those of the 24 optimizations resulting in an f within a factor of 2 of f^*).

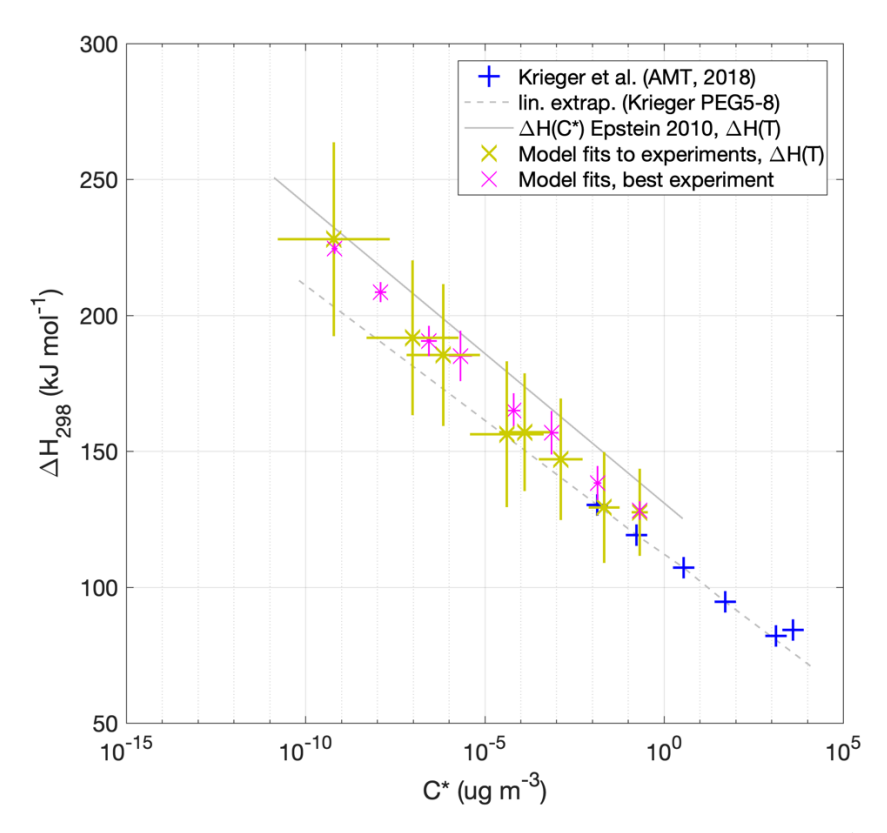


Figure S2: Vaporization enthalpies ΔH vs. saturation vapour concentrations C^* , at 298 K, using the same datasets and colour coding as in Figure S1: based on literature (blue crosses) for PEGs 3-8, and desorption model fits to measurement results in this study for PEGs 7-14 (yellow and magenta crosses, with lines representing uncertainties as discussed in the main text and Figure S1). The grey dashed line indicates a log-linear extrapolation of previously measured C^* and ΔH (PEG5-8; Krieger et al., 2018) up to higher-order PEGs. The solid grey line indicates the empirical relationship ΔH_{298} [kJ mol⁻¹] = 131 – 11 log₁₀(C^*_{298} [μg m⁻³]) proposed by Epstein et al., (2010) based on literature of Antoine coefficients for 821 organic compounds (not including PEGs, except PEG-2).

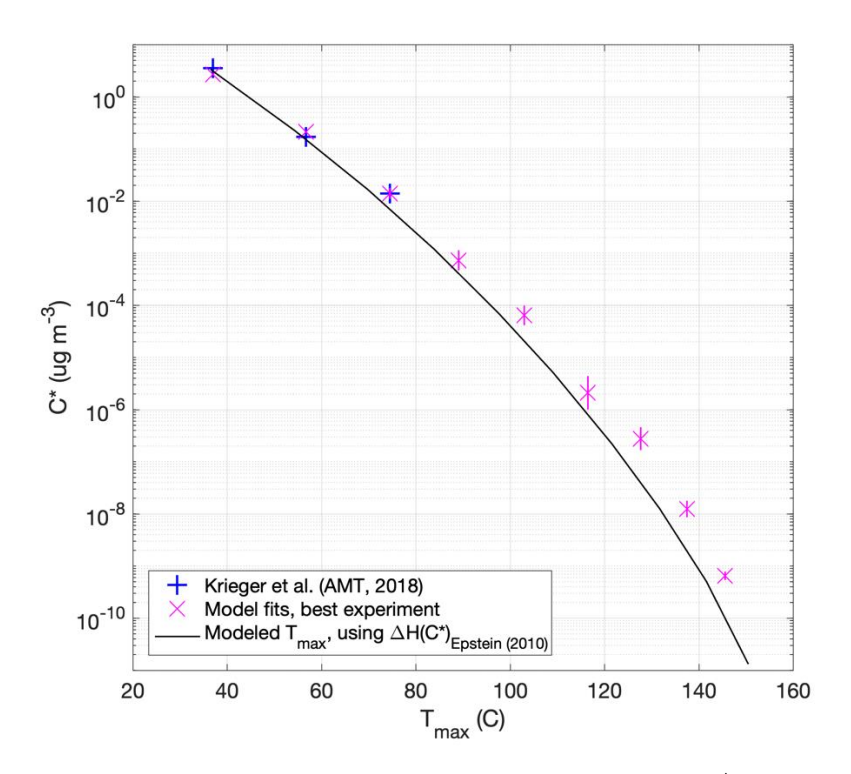


Figure S3: Markers present saturation vapour concentrations C^* for PEGs, at 298 K, using datasets and colour coding as described in Figs. S1 and S2, versus the T_{max} as obtained during the best-fitting experiment (see Fig. S1 for details). The black line presents model simulation results for T_{max} using a series of C^* values in the same range, but using ΔH values obtained via ΔH [kJ mol⁻¹] = 131 – 11 log₁₀(C^* [μg m⁻³]), as proposed by Epstein et al. (2010) based on a broad set of organic compounds. The discrepancy between the line and the markers suggests that if ΔH for PEGs are relatively low (cf. Fig. S2), C^* values assigned to organics that follow the Epstein relationship will be overestimated when assigned based on a T_{max} - C^* relationship established for PEGs. This positive bias increases here with decreasing C^* , up to about an order of magnitude.

Table S2: Measured or estimated P_{sat} values in units of Pa from all introduced measurements and models. The abbreviations used for the methods are explained in the main text (Section 2.3). Two values printed in bold (PEG-9 for K2018, PEG-15 for the desorption model) are estimated based on a log-linear extrapolation of the results for lower-order PEGs. The last row (linear fit) refers to results shown by the dashed line in Figure 2a.

| Method | PEG | PEG-6 | PEG-7 | PEG-8 | PEG-9 | PEG-10 | PEG-11 | PEG-12 | PEG-13 | PEG- | PEG-15 |
|------------|-------------------|---|--------------------|-------------------|--------------------|--------------------|---|--|--|--------------------|--------------------|
| | -5 | | | | | | | | | 14 | |
| K2018 | 5.29 | 3.05 | 1.29 | 9.2 | 3.9 | | | | | | |
| | ×10 ⁻⁴ | ×10 ⁻⁵ | ×10-6 | ×10-8 | ×10 ⁻⁹ | | | | | | |
| L2023 | | 2.24 | 1.06 | 6.51 | 6.71 | | | | | | |
| | | ×10 ⁻⁵ | ×10 ⁻⁶ | ×10 ⁻⁸ | ×10 ⁻⁹ | | | | | | |
| Desorption | | 2.836 ^{+0.518} _{-0.438} | 1.603+1.092 -0.649 | 1.435+2.432 | 7.895+24.397 | 7.003+28.873 | 2.04 ^{+19.682} _{-1.848} | 3.166 ^{+30.225} _{-2.865} | 4.066 ^{+73.924} _{-3.854} | 2.34+85.13 | 1.262+4.2419 |
| model | | ×10 ⁻⁵ | ×10-6 | ×10 ⁻⁷ | ×10 ⁻⁹ | ×10 ⁻¹⁰ | ×10 ⁻¹⁰ | ×10 ⁻¹² | ×10 ⁻¹³ | ×10 ⁻¹⁵ | ×10 ⁻¹⁵ |
| COSMOtherm | 5.3 | 5.47 | | 1.12 | | 9.38 | | 8.73 | | 6.41 | |
| | ×10 ⁻⁴ | ×10 ⁻⁵ | | ×10 ⁻⁷ | | ×10 ⁻¹⁰ | | ×10 ⁻¹² | | ×10 ⁻¹³ | |
| MGM | 2 | 2.28 | 1.91 | 1.5 | 1.19 | 8.97 | 6.55 | 4.65 | 3.21 | 2.16 | 1.42 |
| | ×10 ⁻⁴ | ×10 ⁻⁵ | ×10 ⁻⁶ | ×10 ⁻⁷ | ×10 ⁻⁸ | ×10 ⁻¹⁰ | ×10 ⁻¹¹ | ×10 ⁻¹² | ×10 ⁻¹³ | ×10 ⁻¹⁴ | ×10 ⁻¹⁵ |
| EVAPORATIO | 3.634 | 1.268 | 4.43 | 1.548 | 5.413 | 1.893 | 6.616 | 2.312 | 8.084 | 2.826 | 9.879 |
| N | ×10-5 | ×10 ⁻⁶ | ×10-8 | ×10-9 | ×10 ⁻¹¹ | ×10 ⁻¹² | ×10 ⁻¹⁴ | ×10 ⁻¹⁵ | ×10 ⁻¹⁷ | ×10 ⁻¹⁸ | ×10 ⁻²⁰ |
| | | | | | | | | | | | |

| SIMPOL | 1.276 | 3.204 | 8.048 | 8.049 | 5.078 | 1.305 | 3.355 | 8.428 | 2.167 | 5.444 | 1.399 |
|---------------|-------------------|-------------------|--------------------|--------------------|--------------------|--------------------|--------------------|--------------------|--------------------|--------------------|--------------------|
| | ×10 ⁻⁵ | ×10 ⁻⁷ | ×10 ⁻⁹ | ×10 ⁻¹⁰ | ×10 ⁻¹² | ×10 ⁻¹³ | ×10 ⁻¹⁵ | ×10 ⁻¹⁷ | ×10 ⁻¹⁸ | ×10 ⁻²⁰ | ×10 ⁻²¹ |
| | | | | | | | | | | | |
| M2019 | 1.559 | 5.783 | 2.212 | 8.651 | 3.441 | 1.388 | 5.66 | 2.329 | 9.661 | 4.035 | 1.695 |
| | ×10 ⁻⁶ | ×10 ⁻⁹ | ×10 ⁻¹¹ | ×10 ⁻¹⁴ | ×10 ⁻¹⁶ | ×10 ⁻¹⁸ | ×10 ⁻²¹ | ×10 ⁻²³ | ×10 ⁻²⁶ | ×10 ⁻²⁸ | ×10 ⁻³⁰ |
| | | | | | | | | | | | |
| S2018, | 9.824 | 9.359 | 9.124 | 9.05 | 9.099 | 9.247 | 9.483 | 9.796 | 1.018 | 1.064 | 1.118 |
| monomers | ×10 ⁻⁵ | ×10 ⁻⁷ | ×10 ⁻⁹ | ×10 ⁻¹¹ | ×10 ⁻¹³ | ×10 ⁻¹⁵ | ×10 ⁻¹⁷ | ×10 ⁻¹⁹ | ×10 ⁻²⁰ | ×10 ⁻²² | ×10 ⁻²⁴ |
| | | | | | | | | | | | |
| S2018, | 2.357 | 3.813 | 6.312 | 1.063 | 1.815 | 3.134 | 5.457 | 9.574 | 1.693 | 3 | 5.351 |
| dimers | ×10 ⁻³ | ×10 ⁻⁵ | ×10 ⁻⁷ | ×10 ⁻⁸ | ×10 ⁻¹⁰ | ×10 ⁻¹² | ×10 ⁻¹⁴ | ×10 ⁻¹⁶ | ×10 ⁻¹⁷ | ×10 ⁻¹⁹ | ×10 ⁻²¹ |
| 7.0047 | | | | | | | | | | | |
| L2016 | 3.953 | 1.039 | 2.786 | 7.59 | 2.093 | 5.833 | 1.639 | 4.635 | 1.32 | 3.774 | 1.084 |
| | ×10 ⁻⁴ | ×10 ⁻⁵ | ×10 ⁻⁷ | ×10 ⁻⁹ | ×10 ⁻¹⁰ | ×10 ⁻¹² | ×10 ⁻¹³ | ×10 ⁻¹⁵ | ×10 ⁻¹⁶ | ×10 ⁻¹⁸ | ×10 ⁻¹⁹ |
| P2020 | 3.609 | 8.012 | 1.823 | 4.225 | 9.931 | 2.361 | 5.667 | 1.371 | 3.335 | 8.164 | 2.008 |
| | ×10 ⁻⁶ | ×10 ⁻⁷ | ×10 ⁻⁷ | ×10 ⁻⁸ | ×10-9 | ×10 ⁻⁹ | ×10 ⁻¹⁰ | ×10 ⁻¹⁰ | ×10 ⁻¹¹ | ×10 ⁻¹² | ×10 ⁻¹² |
| | | | | | | | | | | | |
| Linear fit to | 5.287 | 2.677 | 1.39 | 7.344 | 3.938 | 2.136 | 1.17 | 6.449 | 3.58 | 1.999 | 1.121 |
| PEG - number | ×10 ⁻⁴ | ×10 ⁻⁵ | ×10 ⁻⁶ | ×10 ⁻⁸ | ×10-9 | ×10 ⁻¹⁰ | ×10 ⁻¹¹ | ×10 ⁻¹³ | ×10 ⁻¹⁴ | ×10 ⁻¹⁵ | ×10 ⁻¹⁶ |
| | | | | | | | | | | | |
| | | | | | | | | | | | |

Table S3. Measured or estimated C^* values in units of μg m⁻³ and average measured T_{max} values of Experiment A and their standard deviations in units of °C from all introduced measurements and models. The abbreviations used for the methods are explained in the main text (Section 2.3). Two values printed in bold (PEG-9 for K2018, PEG-15 for the desorption model) are estimated based on a log-linear extrapolation of the results for lower-order PEGs. The last row (linear fit) refers to results shown by the dashed line in Figure 2a.

| Method | PEG- | PEG-6 | PEG-7 | PEG-8 | PEG-9 | PEG-10 | PEG-11 | PEG-12 | PEG-13 | PEG-14 | PEG-15 |
|-------------------------|-------|--|---|--|--|--|--|---|--|---|---|
| K2018 | 50.81 | 3.471 | 0.169 | 1.374 ×10 ⁻² | 6.517 ×10 ⁻⁴ | | | | | | |
| L2023 | | 2.607 | 0.138 | 9.364 ×10 ⁻³ | 8.94 ×10 ⁻⁴ | | | | | | |
| Desorption model | | 3.22 ^{+0.589} _{-0.498} | 0.211 ^{+0.144} _{-0.085} | 2.143 ^{+3.632} _{-1.348} ×10 ⁻² | 1.319 ^{+4.076} _{-0.997} ×10 ⁻³ | 1.294 ^{+5.337} _{-1.042} ×10 ⁻⁴ | 4.132 ^{+39,882} ×10 ⁻⁵ | 6.976 ^{+66.611} × 10 ⁻⁷ | 9.684 ^{+176.047} ×10 ⁻⁸ | 6.141 ^{+217.853} ×10 ⁻¹⁰ | 3.446 ^{+116.087} _{-3.347} ×10 ⁻¹⁰ |
| COSMOtherm | 50.91 | 6.226 | | 1.673 ×10 ⁻² | | 1.734 ×10 ⁻⁴ | | 1.924 ×10 ⁻⁶ | | 1.641 ×10 ⁻⁷ | |
| MGM | 19.21 | 2.595 | 0.251 | 2.24 ×10 ⁻² | 1.989 ×10 ⁻³ | 1.658 ×10 ⁻⁴ | 1.327 ×10 ⁻⁵ | 1.025 ×10 ⁻⁶ | 7.645 ×10 ⁻⁸ | 5.528 ×10 ⁻⁹ | 3.886 ×10 ⁻¹⁰ |
| EVAPORATIO N | 3.482 | 0.144 | 5.829 ×10 ⁻³ | 2.312 ×10 ⁻⁴ | 9.045 ×10 ⁻⁶ | 3.449 ×10 ⁻⁷ | 1.341 ×10 ⁻⁸ | 5.096 ×10 ⁻¹⁰ | 1.925 ×10 ⁻¹¹ | 7.232 ×10 ⁻¹³ | 2.704 ×10 ⁻¹⁴ |

| SIMPOL | 1.225 | 3.647 | 1.059 | 1.202 | 8.486 | 2.413 | 6.798 | 1.857 | 5.159 | 1.393 | 3.828 |
|--------------------------|-------|-------------------|-------------------|-------------------|--------------------|--------------------|--------------------|--------------------|--------------------|--------------------|--------------------|
| | | ×10 ⁻² | ×10 ⁻³ | ×10 ⁻⁴ | ×10 ⁻⁷ | ×10 ⁻⁸ | ×10 ⁻¹⁰ | ×10 ⁻¹¹ | ×10 ⁻¹³ | ×10 ⁻¹⁴ | ×10 ⁻¹⁶ |
| | | | | | | | | | | | |
| M2019 | 0.15 | 6.563 | 2.911 | 1.292 | 5.751 | 2.566 | 1.147 | 5.133 | 2.3 | 1.033 | 4.639 |
| | | ×10 ⁻⁴ | ×10-6 | ×10 ⁻⁸ | ×10 ⁻¹¹ | ×10 ⁻¹³ | ×10 ⁻¹⁵ | ×10 ⁻¹⁸ | ×10 ⁻²⁰ | ×10 ⁻²² | ×10 ⁻²⁵ |
| | | | | | | | | - 0 | | | |
| S2018, | 9.437 | 0.107 | 1.201 | 1.352 | 1.521 | 1.71 | 1.922 | 2.16 | 2.427 | 2.725 | 3.06 |
| monomers | | | ×10 ⁻³ | ×10-5 | ×10 ⁻⁷ | ×10 ⁻⁹ | ×10 ⁻¹¹ | ×10 ⁻¹³ | ×10 ⁻¹⁵ | ×10 ⁻¹⁷ | ×10 ⁻¹⁹ |
| | | | | | | | | | | | |
| S2018, dimers | 226.4 | 4.34 | 8.306 | 1.588 | 3.034 | 5.793 | 1.106 | 2.11 | 4.025 | 7.678 | 1.464 |
| | | | ×10 ⁻² | ×10 ⁻³ | ×10 ⁻⁵ | ×10 ⁻⁷ | ×10 ⁻⁸ | ×10 ⁻¹⁰ | ×10 ⁻¹² | ×10 ⁻¹⁴ | ×10 ⁻¹⁵ |
| | | | | | | | | | | | |
| L2016 | 37.97 | 1.182 | 3.666 | 1.134 | 3.498 | 1.078 | 3.32 | 1.022 | 3.142 | 9.657 | 2.967 |
| | 1 | | ×10 ⁻² | ×10 ⁻³ | ×10 ⁻⁵ | ×10 ⁻⁶ | ×10 ⁻⁸ | ×10 ⁻⁹ | ×10 ⁻¹¹ | ×10 ⁻¹³ | ×10 ⁻¹⁴ |
| | | | | | | | | | | | |
| P2020 | 0.347 | 9.12 | 2.398 | 6.3 | 1.659 | 4.365 | 1.148 | 3.02 | 7.943 | 2.089 | 5.495 |
| | | ×10 ⁻² | ×10 ⁻² | ×10 ⁻³ | ×10 ⁻³ | ×10 ⁻⁴ | ×10 ⁻⁴ | ×10 ⁻⁵ | ×10-6 | ×10-6 | ×10 ⁻⁷ |
| | | | | | | | | | | | |
| Linear fit to | 50.78 | 3.048 | 0.1828 | 1.097 | 6.581 | 3.948 | 2.368 | 1.421 | 8.526 | 5.115 | 3.069 |
| PEG-number | 7 | | | ×10 ⁻² | ×10 ⁻⁴ | ×10 ⁻⁵ | ×10-6 | ×10 ⁻⁷ | ×10-9 | ×10 ⁻¹⁰ | ×10 ⁻¹¹ |
| | | | | | | | | | | | |
| Average T _{max} | 21.3 | 39.2 ± | 59.16 ± | 76.36 ± | 91.62 ± | 106 ± | 118.87 ± | 130.4 ± | 140.29 ± | 148.17 ± | 153.94 ± |
| values + std | ± | 3.74 | 3.6 | 3.45 | 3.83 | 3.74 | 3.74 | 3.62 | 3.71 | 3.41 | 3.66 |
| shown in | 2.05 | | | | | | | | | | |
| Figure 1 and | | | | | | | | | | | |
| Figure 2 | | | | | | | | | | | |

110

Table S4: Desorption model-derived values for vaporization enthalpy ΔH in units of kJ mol⁻¹, including uncertainties.

| | PEG-7 | PEG-8 | PEG-9 | PEG-10 | PEG-11 | PEG-12 | PEG-13 | PEG-14 |
|------------|---------------|-----------|-----------|-----------|-----------|-----------|-----------|----------|
| ΔH | $127.553 \pm$ | 129.312 ± | 147.042 ± | 157.032 ± | 156.265 ± | 185.414 ± | 191.754 ± | 228.01 ± |
| | 16.022 | 20.383 | 22.366 | 21.67 | 26.843 | 26.096 | 28.463 | 35.661 |

5 References

- Epstein, S. A., Riipinen, I., & Donahue, N. M. (2010). A semiempirical correlation between enthalpy of vaporization and saturation concentration for organic aerosol. *Environmental Science and Technology*, 44(2), 743–748. https://doi.org/10.1021/ES902497Z/SUPPL FILE/ES902497Z SI 001.PDF
- Hyttinen, N., & Prisle, N. L. (2020). Improving Solubility and Activity Estimates of Multifunctional Atmospheric Organics by Selecting Conformers in COSMO therm. *Journal of Physical Chemistry A*, 124(23), 4801–4812. https://doi.org/10.1021/ACS.JPCA.0C04285/ASSET/IMAGES/LARGE/JP0C04285_0002.JPEG
 - KIT SCC Dienste Softwarekatalog TURBOMOLE. Retrieved April 8, 2025, from https://www.scc.kit.edu/produkte/turbomole.php
 - Krieger, U. K., Siegrist, F., Marcolli, C., Emanuelsson, E. U., Gøbel, F. M., Bilde, M., Marsh, A., Reid, J. P., Huisman, A. J., Riipinen, I., Hyttinen, N., Myllys, N., Kurtén, T., Bannan, T., Percival, C. J., & Topping, D. (2018). A reference data set for validating vapor pressure measurement techniques: Homologous series of polyethylene glycols. *Atmospheric Measurement Techniques*, 11(1), 49–63. https://doi.org/10.5194/amt-11-49-2018
 - Kurtén, T., Hyttinen, N., Louise D'Ambro, E., Thornton, J., & Prisle, N. L. (2018). Estimating the saturation vapor pressures of isoprene oxidation products C5H12O6 and C5H10O6 using COSMO-RS. *Atmospheric Chemistry and Physics*, 18(23), 17589–17600. https://doi.org/10.5194/ACP-18-17589-2018

Li, Z., Buchholz, A., Barreira, L. M. F., Ylisirniö, A., Hao, L., Pullinen, I., Schobesberger, S., & Virtanen, A. (2023). Isothermal evaporation of α-pinene secondary organic aerosol particles formed under low NOx and high NOx conditions. *Atmospheric Chemistry and Physics*, 23(1), 203–220. https://doi.org/10.5194/ACP-23-203-2023

BIOVIA COSMOtherm: Release 2021, Dassault Systèmes, available at: http://www.3ds.com, last access: 1 April 2021